The Distance to the Stars

Ralf Siebenmorgen[1] and Rolf Chini[2]

[1] European Southern Observatory, Karl-Schwarzschild-Str. 2, 85748 Garching, Germany,
email: Ralf.Siebenmorgen@eso.org

[2] Ruhr University Bochum, Faculty of Physics and Astronomy, Astronomical Institute (AIRUB), 44780 Bochum, Germany; Universidad Catolica del Norte, Instituto de Astronomia, Avenida Angamos 0610, Antofagasta, Chile; Nicolaus Copernicus Astronomical Center of the Polish Academy of Sciences, Bartycka 18, 00-716 Warsaw, Poland

Abstract

The vastness of a clear night sky evokes for most people curiosity about the distance to the stars. There are two primary methods for estimating stellar distances – parallax and luminosity. In this study, we present a new analysis revealing a noteworthy discrepancy between these two methods. Due to the accuracy of GAIA, parallaxes can directly be converted into distances. In contrast, luminosity distances require – apart from the determination of apparent and absolute brightness of a star – the reddening value that allows a correction for interstellar extinction. Using 47 stars with non-peculiar reddening curves from the high-quality sample[1] we find here that the luminosity distance overestimates the parallactic distance for most (80%) of these stars. This puzzling discrepancy can only be removed when incorporating a new population of large dust grains – so called *dark dust* – with our model[2] that respects contemporary constraints of the inter-stellar dust[3] and is updated to scope for the first time with the absolute reddening. The model provides a visual extinction which unifies the conflicting distances. Another far reaching consequence of the flat absorption and scattering properties of dark dust is that it broadens the light curves[4] of SN Ia, which serve as a measure of the quantity of dark energy[5].

1. Parallax and luminosity distance

The distance measurement to stars has long intrigued astronomers, prompting the exploration of various estimation techniques. Parallax, based on geometric principles, provides a straightforward approach but is limited to nearby stars whereas luminosity distance $D_{\rm L}$ estimates enable the assessment of distances of several kpc. However, the extinction by dust diminishes the apparent brightness of stars and requires a precise determination. We examine 47 prominent OB stars within a distance of 2.5 kpc with the most superior sample of reddening curves currently accessible[1]. These stars have undergone precise spectral classifications through high-resolution spectroscopy with UVES[6] at resolving power $\lambda/\Delta\lambda \sim 75,000$) and their accurate distances have been obtained using the unprecedented precision of the GAIA[7] parallax at $\sigma < 0.1$ mas. For many stars, our investigation uncovers a substantial inconsistency between both classical derivations of stellar distances.

The paradox in the distance estimates remained undetected until now and its detection required the unprecedented resolution of the GAIA data release three[7].

By introducing the photometric equation nearly 100 years ago it was speculated that an additional non-selective or grey extinction term in the form of very large grains – at that time called 'meteoritic' bodies – might exist[8]. For a few stars it was hypothesized[9,10] that incorporating such an additional dust component could reconcile the disparity between distance estimates; however, this remained unverified due to the lack of a physical dust model. To reconcile the observed discrepancy, we introduce a new method to determine the visual extinction. It considers both the influence of micron-sized grains as a new population in the ISM and the distance provided by GAIA as a so far unused constraint in dust models.

2. The sample

The reddening curves were scrutinized by excluding stars with composite spectra in the IUE[11,12] / FUSE[13] aperture due to multiple bright stellar systems, inconsistent parallaxes between data releases two[14] and three[7] from GAIA, uncertain spectral type designations or photometric variability. In addition, the current investigation requires precise absolute stellar brightness $M_{\rm V}$. Therefore, we dropped three Be stars due to possible variability. Another three stars with peculiarities in their reddening curves were also omitted decreasing the total number of the sample to 47 stars. To compensate for the binarity of five stars[15−19] we added the absolute brightness of the corresponding two components.

3. Dark dust model

Our study utilizes a dust model[2] that aligns with current observational constraints of dust in the diffuse ISM of the Milky Way[3]. It accounts for representative solid phase element abundances and explains accurately phenomena such as wavelength dependent reddening, extinction, starlight polarization, and the emission of polarized and unpolarized light. In addition, it accounts for the increased submm/mm emission observed by Planck and explains the polarized emission seen by Planck[20].

The model[2] incorporates three dust populations: 1) nanoparticles of graphite, silicate, and polycyclic aromatic hydrocarbon (PAH), 2) submicrometre sized spheroidal grains of amorphous carbon and silicate, using the latest optical constants for amorphous silicates[21], and 3) micrometre sized dust particles. The latter dust component, proposed by[10] has been labelled as dark dust. The micrometre sized grains are primarily composed as a composite of porous amorphous carbon and silicate particles. Micrometre sized grains have been detected in scattering light haloes around X-ray sources[22,23] from submillimeter emission of evolved giants[24]. They preferentially survive the interaction regions between the asymptotic giant branch and the ISM[25]. Micrometre sized particles from the diffuse ISM were also measured in-situ from the Ulysses, Galileo, and Stardust space probes[26−28]. This hidden dust component appears in sightlines that are connected to the cold ISM[10].

Micrometre sized grains absorb a fraction of the interstellar radiation field, ISRF[29]. Because these grains are large, they are cold and will emit at long wavelengths. Originally very cold (10 K) dust emission was detected in our Galaxy towards high density regions[30] and in non-active galaxies[31]. Such cold dust was confirmed with ISO[32,33], and more recently, observed excess emission at 0.5 mm with Herschel that cannot be explained by a single modified black-body temperature component[34–36]; these results were confirmed with ALMA[37] and LABOCA[38] at even longer wavelengths.

4. Distance discrepancy

We observed a discrepancy between the distances obtained from luminosity and from parallax. In Fig. 1 we show the distance ratios $D_{\mathrm{L}}/D_{\mathrm{GAIA}}$ vs. D_{GAIA} for our sample. For the same star the luminosity distance D_{L} generally overpredicts the distance D_{GAIA} derived from the GAIA parallax. The luminosity distance is computed using Hipparcos photometry[39] and spectral types from UVES[1]. Absolute magnitudes M_{V} were calculated from our spectral types and the conversion tables[40,41]. Visual extinctions A_{V} were extracted from published reddening curves[11–13]. A dependency of D_{L} on the spectral types and luminosity classes of the stars is not observed.

The (sub)millimetre excess emission observed in the Milky Way has gained explanation only recently. In alternative models, this phenomenon is attributed to the adjustment of grain emissivity at these wavelengths[3,20]. These authors avoid a population of micrometre sized cold dust. However, these models fail short resolving the distance discrepancy observed in this work towards individual stars (Fig. 1).

5. Absolute reddening

By analysing the spectral type and luminosity class of a star one finds the absolute magnitude M_{V} and with available photometry, one establishes the reddening $E(B-V)$. We calculate the visual extinction A_{V} necessary to align the luminosity distance precisely with the distance D_{GAIA} derived from GAIA data using the photometric equation:

$$A_{\mathrm{V}} = V - M_{\mathrm{V}} - 5\log D_{\mathrm{GAIA}} + 5\,. \tag{1}$$

The optical depth $\tau_V = A_{\mathrm{V}}/1.086$ is related to the column densities of nanoparticles and submicrometre sized particles N_n and to the column density of the new dust component of micrometre sized grains N_μ, with corresponding mass extinction cross-section K_n and K_μ (g/cm^3) based on the dust model[2]:

$$\tau_V = N^n\, K^n_V \;+\; N^\mu\, K^\mu_V \;<\; \|E(H)\|\,/1.086\,. \tag{2}$$

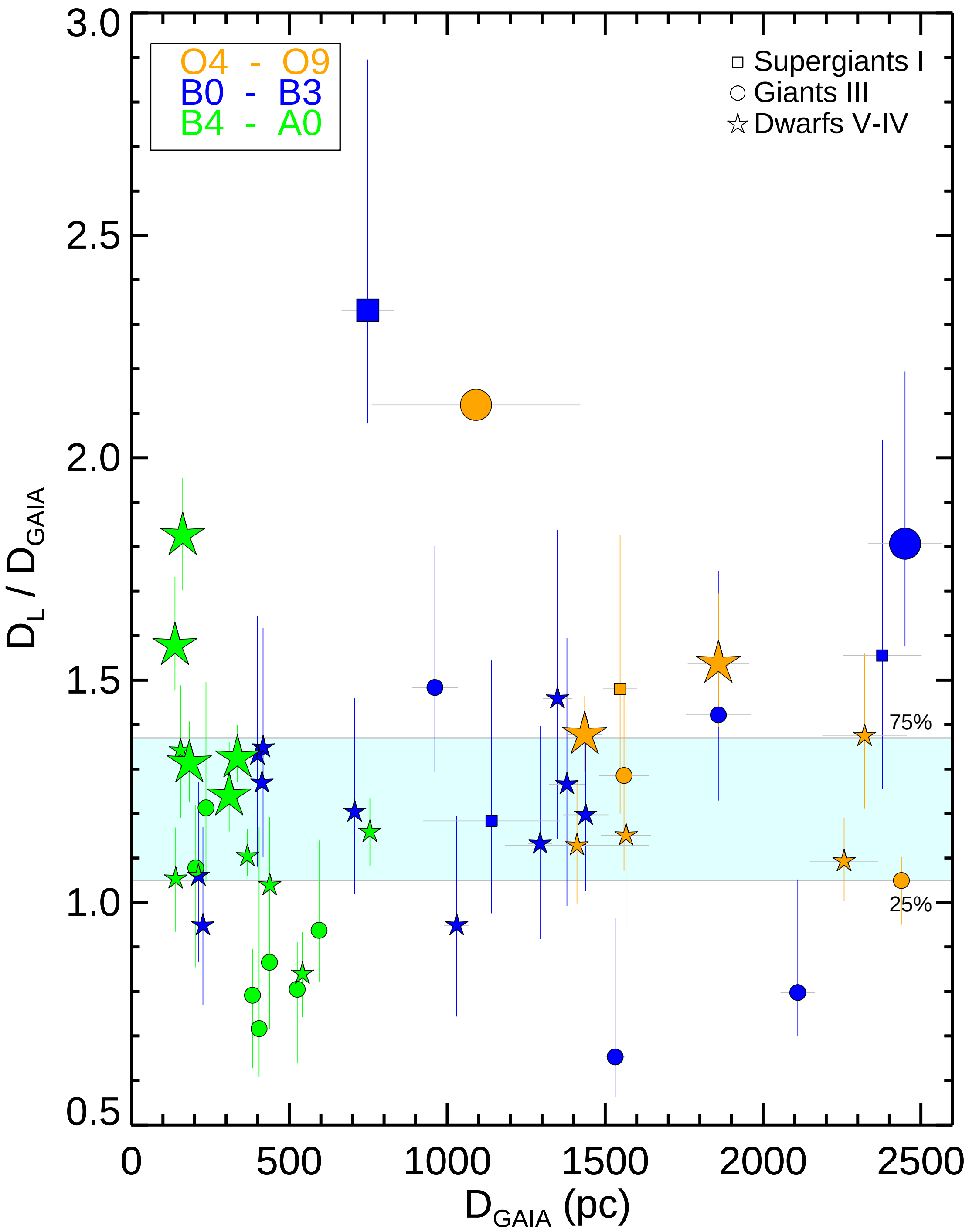

Fig. 1. The distance discrepancy. The distance ratios $D_{\rm L}/D_{\rm GAIA}$ vs. $D_{\rm GAIA}$ (7) for our sample of 47 stars with the most accurate reddening curves[1]. The distance ratios range between 0.65 and 2.33 and show a 1σ scatter of 0.33 at a median of 1.2. The area between the bottom and top quartiles at 1.05 and 1.35 is shown in cyan and underlines the overprediction in $D_{\rm L}$. The error bars in $D_{\rm L}$ primarily arise from systematic uncertainties in the $M_{\rm V}$ determination. Specifically, the uncertainties in $M_{\rm V}$ are quantified as the 1σ scatter between the $M_{\rm V}$ values of the spectral type and luminosity class and those of the adjacent ±0.5 subtype σ_{SpT} and ±1 luminosity class σ_{LC} and an offset between the catalogues[40,41] σ_C, using $\sigma^2 = \sigma^2_{SpT} + \sigma^2_{LC} + \sigma^2_C$ (see Appendix). Different symbols and colours are used to visually represent the various spectral types and luminosity classes as labelled. Stars with a deviation in the distance ratios from unity that are below 3σ are shown by small and the other 10 stars with confidence above 3σ by large symbols, respectively. There are no stars with a distance ratio below $D_{\rm L}/D_{\rm GAIA} < 1.2$ detected at high 3σ confidence.

The extinction cross-section[42–44] diminishes at infinite wavelengths, $K(\infty) = 0$. To prevent negative optical depths, we assume that the reddening at infinite wavelengths is smaller than in the H-band, hence $A_{\rm V} = -E(\infty) > -E(H)$. The reddening $E(B-V) = 1.086\ (\tau_B - \tau_V)$ provides a second constraint:

$$\tau_B - \tau_V = N^n\ (K_B^n - K_V^n)\ +\ N^\mu\ (K_B^\mu - K_V^\mu)\ . \tag{3}$$

These two equations enable us to derive the specific mass of each component, specifically $m_n = N_n/(N_n + N_\mu)$ of the nano- and submicrometre grains and $m_\mu = N_\mu/(N_n + N_\mu)$ of the micrometre sized particles. The normalized reddening curves are converted into absolute reddening by multiplying $E(B-V)$. The extrapolated reddening at infinitely long wavelengths is substituted with the visual extinction $A_{\rm V}$ (Eq. 1). Notably, our approach obviates the requirement for the extrapolated parameter $R_{\rm V} = A_{\rm V}/E(B-V)$ (45). By adjusting grain sizes and abundances within the three populations, we achieve the best fit for the absolute reddening of each star, surpassing previous models that solely addressed relative reddening or extinction curves.

6. Methods

The methodology for calculating the extinction cross-section (K) for partially aligned and wobbling spheroidal grains, nanoparticles, and PAH, from the optical constants of dust materials, is outlined in (2). The normalized reddening curves $E(\lambda - {\rm V})/{\rm E(B-V)}$ for the sample are sourced from the references listed in column 5 of Table 1. These curves are transformed into absolute reddening that are used in this work by multiplying them with the corresponding reddening $E(B-V)$ provided in those same references. The extrapolated reddening at infinitely long wavelengths is substituted with the visual extinction (A_V), derived from Eq. 1, and are specified in column 10 of Table 1. Notably, our approach obviates the requirement for the extrapolated parameter $R_V = A_V/E(B-V)$.

For achieving the optimal fits, we employ the vectorized minimum χ^2 fitting procedure by (2). In this context, the specific masses of various particles are treated as free parameters: the micrometer sized grains (m_μ), submicrometer sized particles composed of amorphous silicates ($m_{\rm Si}$) and carbon ($m_{\rm aC}$), and the nanoparticles of silicates ($m_{\rm vSi}$), graphite ($m_{\rm vgr}$), and PAH ($m_{\rm PAH}$). These fits adhere to the constraint of cosmic solid phase abundances, ensuring [C]/[Si]< 5.2.

Fine tuning of the fits to the 2175 Å bump involves allowing the central wavelength (x_0) and damping constant (γ) of the Lorentzian profiles of PAH absorption cross-section to remain free. In the framework of the power-law dust size distribution, the exponent (q) and upper radii for micrometer sized (r_μ^+), submicrometer sized silicate, and carbon grains ($r_{\rm Si}^+$, $r_{\rm aC}^+$) are treated as adjustable parameters. The details of the model parameters, along with their reduced χ_r^2 values for the best fit, are summarized in Table 2 (see Appendix) and fits are show in Fig. 2.

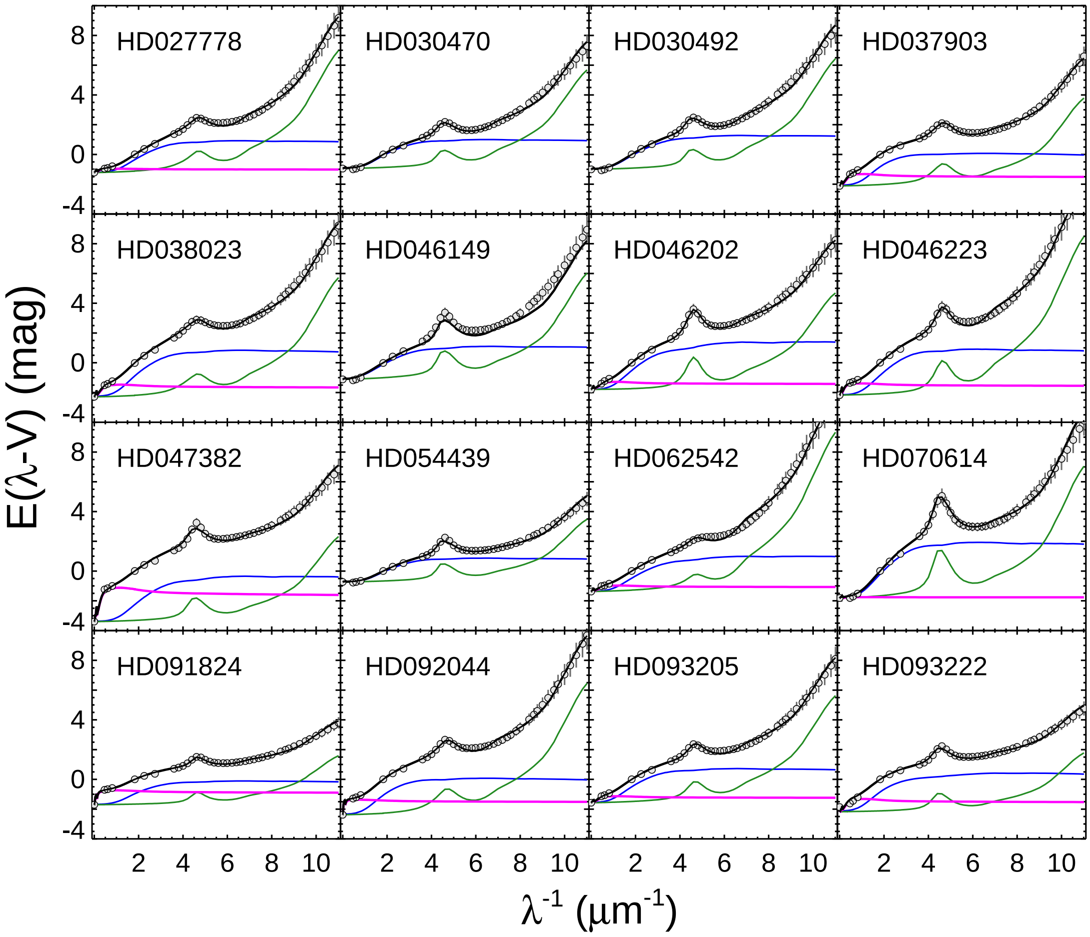

Fig. 2. Display of the absolute reddening (symbols) corresponding to individual stars. These values are complemented by the optical depth $A_V = -E(\infty)$, which is calculated using Eq. 1. The model (black) with contributions from the nanoparticles (green), submicron (blue) and micron sized grains (magenta) are shown.

7. Distance unification

The proposed model effectively resolves the distance discrepancy brought here to light utilizing the unprecedented resolution of the GAIA data release three. Recent investigations[46] were still not able to detect any discrepancy within the errors of the GAIA data release two[14]. In this manner, we achieve a consistent estimate of the absolute reddening $E(\lambda - V)$ going beyond previous models that only discussed normalized reddening $E(\lambda - V)/E(B - V)$.

In Fig. 3 we compute the luminosity distance by determining A_V from the photometric equation with D_{GAIA} as input. The reliability of our A_V estimate (Eq. 1) is confirmed by fitting the absolute reddening curve towards the stars using our dust model, which incorporates micrometre sized grains. Only for seven sightlines, a satisfactorily fit can be achieved without the new population of micrometre sized particles. The scatter in our distance ratio (Fig. 3) is reduced by a factor

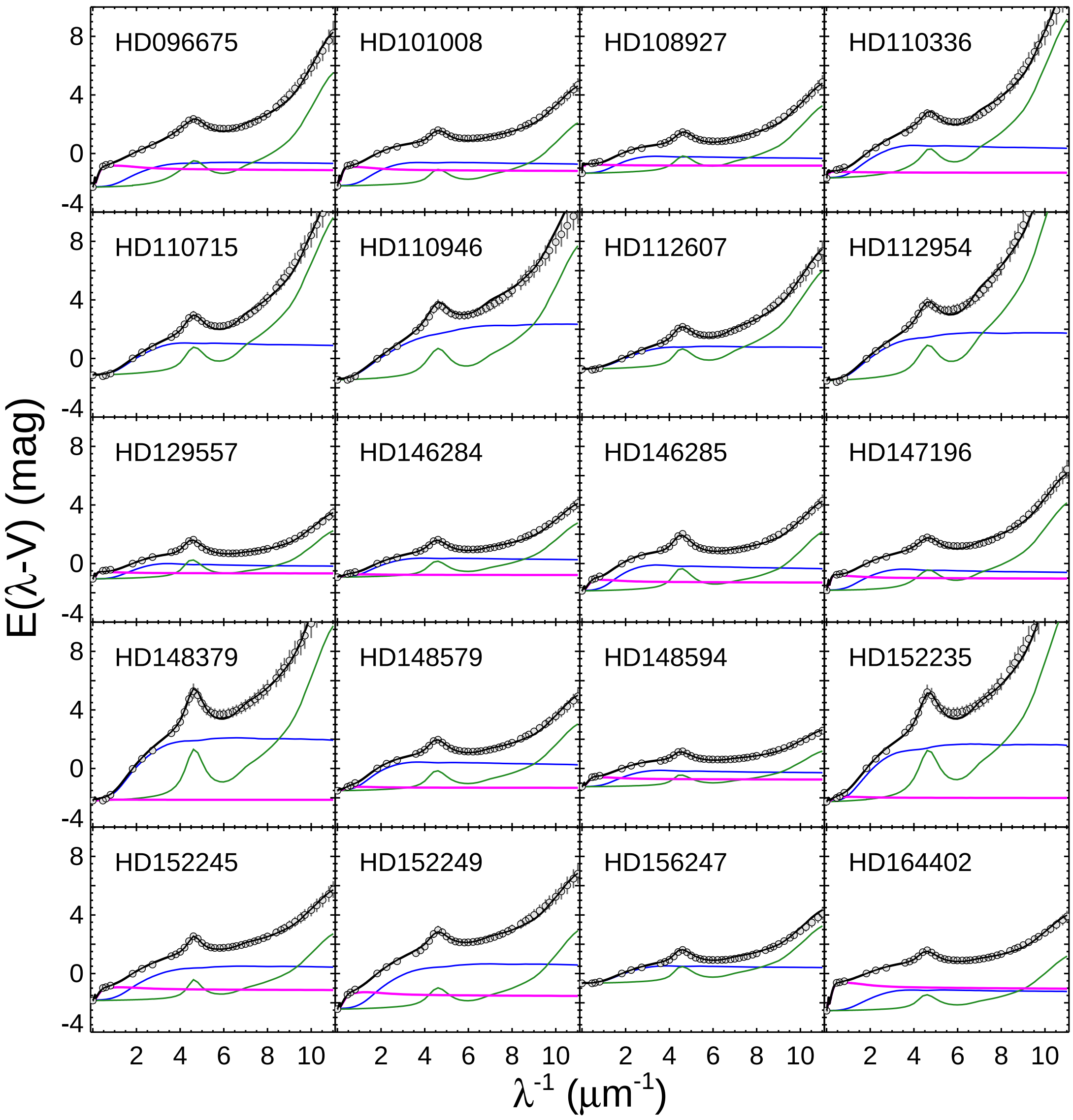

Fig. 2. – continued –

5.5 when compared to the literature values and compensates for the overprediction of previous estimates (Fig. 1).

8. Conclusion

Our distance analysis for bright stars uncovers a significant discrepancy between parallax and luminosity distance measurements for 79% of the objects. To resolve this distance paradox, we propose a physically consistent dust model incorporating micrometre sized grains as a new, so far hidden population of dust particles in the general field of the ISM, and an estimate of the visual extinction towards the star derived from the GAIA parallax. By accounting for these aspects, we successfully

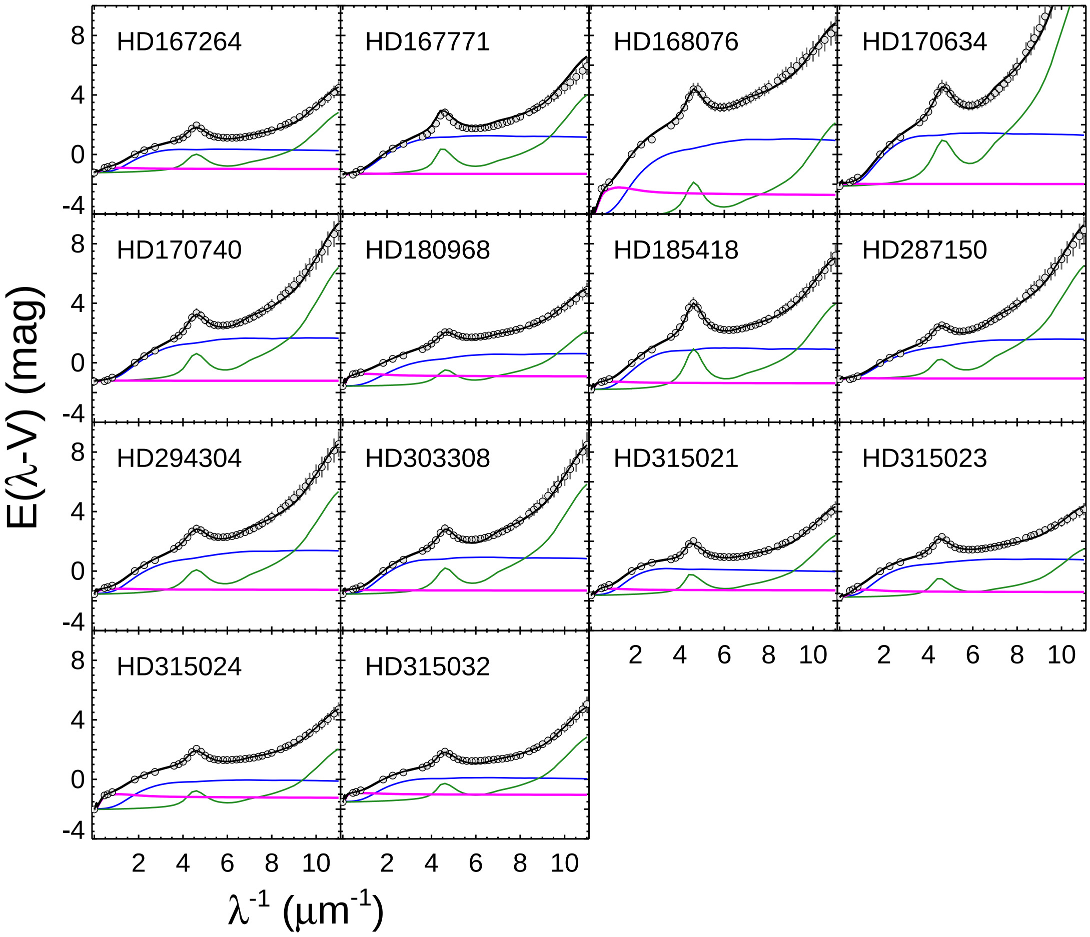

Fig. 2. – continued –

reconcile the observed disagreement and present a unified approach for stellar distance estimation. This study emphasizes the significance of considering the absolute reddening of individual sight-lines when deriving parameters like R_V and underscores the necessity for further investigations of large dust particles in stellar distance determination.

Dark dust induces a wavelength independent extinction from the far UV to the near infrared which makes it invisible for standard photometric methods to determine interstellar extinction. This new dust component significantly influences various aspects of the grain physics of the ISM. Along with its scattering properties[47,48], such a dust component in the vicinity of SNIa progenitors will contribute to the broadening of SN Ia light curves[4,49], which has even implications for our understanding of the quantity of dark energy present in the universe[5].

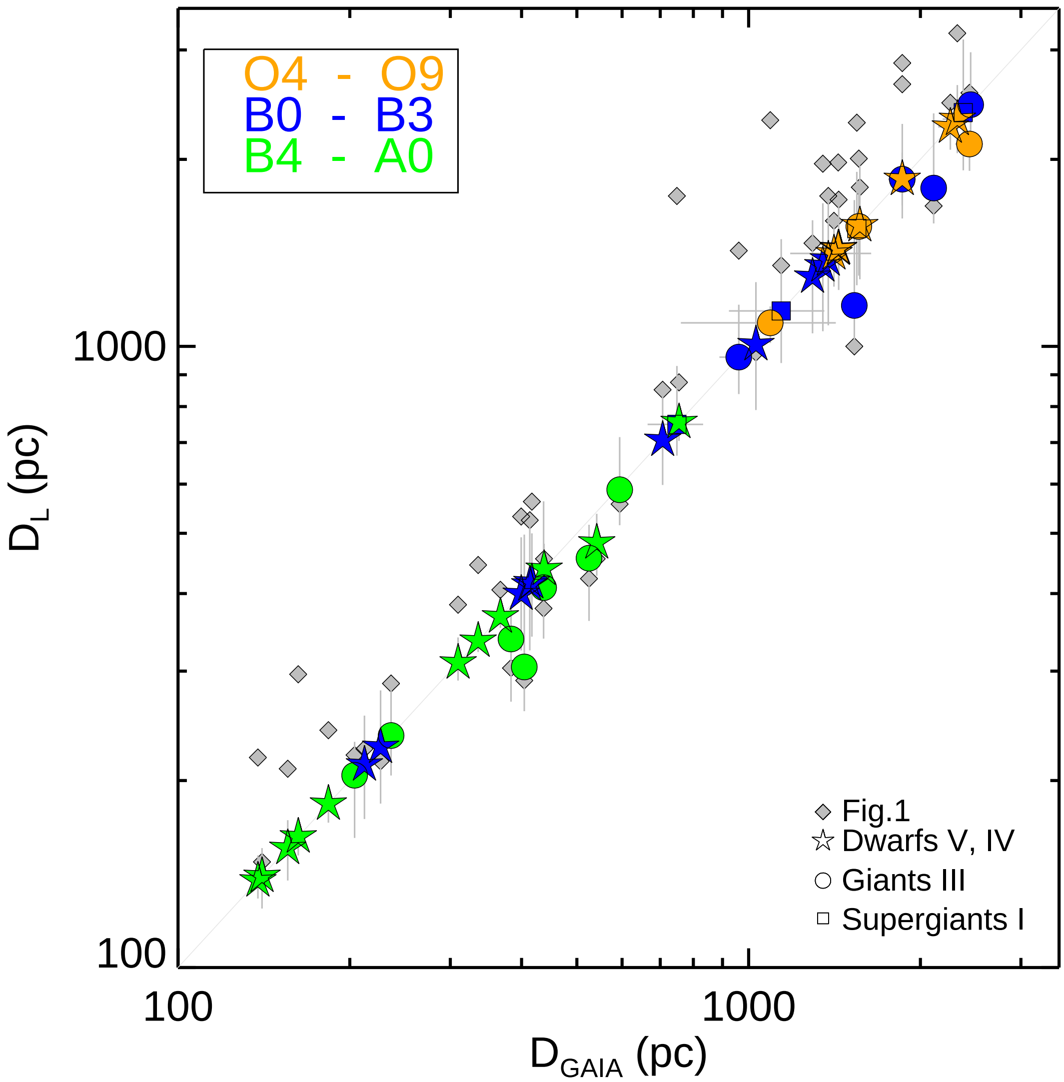

Fig. 3. The unification of luminosity and parallax distances. Our estimate of the luminosity distances $D_{\rm L}$ agrees with the parallax distances $D_{\rm GAIA}$ (7) for 37 out of 47 stars to better than 1%. The distance ratio $D_{\rm L}/D_{\rm GAIA}$ ranges between 0.75 and 1.0 and shows a 1σ scatter of 6% around a median of 1. Spectral types and luminosity classes are denoted as in Fig. 1.

9. References

1. Siebenmorgen, R., Smoker, J., Krelowski, J., Gordon, K., Chini, R. Dark Dust III: The high-quality single-cloud reddening curve sample. Scrutinizing extinction curves in the Milky Way, A&A 676A, 132 (2023).
2. Siebenmorgen, R., Dark dust. II. Properties in the general field of the diffuse ISM, Astronomy and Astrophysics, 670, A115 (2023).
3. Hensley, B. S., Draine, B. T. Observational Constraints on the Physical Properties of Interstellar Dust in the Post-Planck Era, The Astrophysical Journal, 906, 73 (2021).
4. Krügel, E. Photometry of variable dust enshrouded stars. Supernovae Ia, Astronomy and Astrophysics, 574, A8 (2015).

5. Riess, A. G., Observational Evidence from Supernovae for an Accelerating Universe and a Cosmological Constant, The Astronomical Journal, 116, 1009-1038 (1998).
6. Dekker, H., D'Odorico, S., Kaufer, A., Delabre, B., Kotzlowski, H. Design, construction, and performance of UVES, the echelle spectrograph for the UT2 Kueyen Telescope at the ESO Paranal Observatory, Optical and IR Telescope Instrumentation and Detectors, 4008, 534-545 (2000).
7. GAIA Collaboration GAIA Data Release 3. The extragalactic content, Astronomy and Astrophysics, 674, A41 (2023).
8. Trumpler, R. J. Spectrophotometric Measures of Interstellar Light Absorption, Publications of the Astronomical Society of the Pacific, 42, 267 (1930).
9. Krelowski, J., Galazutdinov, G. A., Strobel, A., Mulas, G. Gray Extinction in the Orion Trapezium, Acta Astronomica, 66, 469-480 (2016).
10. Siebenmorgen, R., Krelowski, J., Smoker, J., Galazutdinov, G., Bagnulo, S. Dark dust and single-cloud sightlines in the ISM, Astronomy and Astrophysics, 641, A35 (2020).
11. Valencic, L. A., Clayton, G. C., Gordon, K. D. Ultraviolet Extinction Properties in the Milky Way, The Astrophysical Journal, 616, 912-924 (2004).
12. Fitzpatrick, E. L., Massa, D. An Analysis of the Shapes of Interstellar Extinction Curves. V. The IR-through-UV Curve Morphology, The Astrophysical Journal, 663, 320-341 (2007).
13. Gordon, K. D., Cartledge, S., Clayton, G. C. FUSE Measurements of Far-Ultraviolet Extinction. III. The Dependence on R(V) and Discrete Feature Limits from 75 Galactic Sightlines, The Astrophysical Journal, 705, 1320-1335 (2009).
14. GAIA Collaboration GAIA Data Release 2. Summary of the contents and survey properties, Astronomy and Astrophysics, 616, A1 (2018).
15. Mahy, L., et al. Early-type stars in the young open cluster NGC 2244 and in the Monoceros OB2 association. I. The multiplicity of O-type stars. Astronomy and Astrophysics, 502, 937-950 (2009)
16. Sota, A., et al. The Galactic O-Star Spectroscopic Survey (GOSSS). II. Bright Southern Stars,The Astrophysical Journal Supplement Series, 211, 10 (2014).
17. Bozkurt, Z., Değirmenci, Ö. L. Triple systems showing apsidal motion, Monthly Notices of the Royal Astronomical Society, 379, 370-378 (2007).
18. Mahy, L., et al. Identifying quiescent compact objects in massive Galactic single-lined spectroscopic binaries, Astronomy and Astrophysics, 664, A159 (2022).
19. Maíz Apellániz, J., et al. MONOS: Multiplicity Of Northern O-type Spectroscopic systems. I. Project description and spectral classifications and visual multiplicity of previously known objects,Astronomy and Astrophysics,626, A20 (2019).
20. Guillet, V., et al. Dust models compatible with Planck intensity and polarization data in translucent lines of sight, Astronomy and Astrophysics, 610, A16 (2018).
21. Demyk, K., et al. Low-temperature optical constants of amorphous silicate dust analogues, Astronomy and Astrophysics, 666, A192 (2022).

22. Witt, A. N., Smith, R. K., Dwek, E. X-Ray Halos and Large Grains in the Diffuse Interstellar Medium, The Astrophysical Journal, 550, L201-L205 (2001).
23. Heinz, S., et al. A Joint Chandra and Swift View of the 2015 X-ray Dust scattering Echo of V404 Cygni, The Astrophysical Journal, 825, 15 (2016).
24. Jura, M., Webb, R. A., Kahane, C. Large Circumbinary Dust Grains around Evolved Giants?, The Astrophysical Journal, 550, L71-L75 (2001).
25. Maercker, M., Khouri, T., Mecina, M., De Beck, E. Investigating dust properties in AGB wind-ISM interaction regions, Astronomy and Astrophysics, 663, A64 (2022).
26. Landgraf, M., Baggaley, W. J., Grün, E., Krüger, H., Linkert, G. Aspects of the mass distribution of interstellar dust grains in the solar system from in situ measurements, Journal of Geophysical Research, 105, 10343-10352 (2000).
27. Westphal, A. J., et al. Evidence for interstellar origin of seven dust particles collected by the Stardust spacecraft, Science, 345, 786-791 (2014).
28. Krüger, H., Strub, P., Grün, E., Sterken, V. J. Sixteen Years of Ulysses Interstellar Dust Measurements in the Solar System. I. Mass Distribution and Gas-to-dust Mass Ratio, The Astrophysical Journal, 812, 139 (2015).
29. Mathis, J. S., Mezger, P. G., Panagia, N. Interstellar radiation field and dust temperatures in the diffuse interstellar medium and in giant molecular clouds, Astronomy and Astrophysics, 128, 212-229 (1983).
30. Chini, R., et al. Discovery of a cold and gravitationally unstable cloud fragment., Astronomy and Astrophysics, 272, L5-L8 (1993).
31. Chini, R., Kruegel, E., Lemke, R., Ward-Thompson, D. Dust in spiral galaxies. II., Astronomy and Astrophysics, 295, 317-329 (1995).
32. Krugel, E., Siebenmorgen, R., Zota, V., Chini, R. ISOPHOT boosts dust masases in spiral galaxies, Astronomy and Astrophysics, 331, L9-L12 (1998).
33. Siebenmorgen, R., Krügel, E., Chini, R. Very cold dust in galaxies, Astronomy and Astrophysics, 351, 495-505 (1999).
34. Madden, S. C., et al An Overview of the Dwarf Galaxy Survey, Publications of the Astronomical Society of the Pacific, 125, 600 (2013).
35. Kennicutt, R. C., et al. KINGFISH—Key Insights on Nearby Galaxies: A Far-Infrared Survey with Herschel: Survey Description and Image Atlas, Publications of the Astronomical Society of the Pacific, 123, 1347 (2011).
36. Rémy-Ruyer, A., et al. Revealing the cold dust in low-metallicity environments. I. Photometry analysis of the Dwarf Galaxy Survey with Herschel, Astronomy and Astrophysics, 557, A95 (2013).
37. Galliano, F., Madden, S. C., Jones, A. P., Wilson, C. D., Bernard, J.-P. ISM properties in low-metallicity environments. III. The spectral energy distributions of II Zw 40, He 2-10 and NGC 1140, Astronomy and Astrophysics, 434, 867-885 (2005).

38. Galametz, M., et al. Probing the dust properties of galaxies up to submillimetre wavelengths. I. The spectral energy distribution of dwarf galaxies using LABOCA, Astronomy and Astrophysics, 508, 645-664 (2009).
39. Kharchenko, N. V., Roeser, S. VizieR Online Data Catalog: All-Sky Compiled Catalogue of 2.5 million stars (Kharchenko+ 2009), VizieR Online Data Catalog, I/280B (2009).
40. Bowen, D. V., et al. The Far Ultraviolet Spectroscopic Explorer Survey of O VI Absorption in the Disk of the Milky Way, The Astrophysical Journal Supplement Series, 176, 59-163 (2008).
41. Wegner, W. Absolute magnitudes of OB and Be stars based on Hipparcos parallaxes - III, Monthly Notices of the Royal Astronomical Society, 374, 1549-1556 (2007).
42. Draine, B. T. Interstellar dust grains. Ann. Rev. Astron. Astrophys. 41, 241-289 (2003).
43. Voshchinnikov, N. V. Optics of cosmic dust I, Astrophysics and Space Physics Reviews, 12, 1 (2004).
44. Krügel, E. An introduction to the physics of interstellar dust, An introduction to the physics of interstellar dust, IoP (2008).
45. Gordon, K. D., et al. One Relation for All Wavelengths: The Far-ultraviolet to Mid-infrared Milky Way Spectroscopic R(V)-dependent Dust Extinction Relationship, The Astrophysical Journal, 950, 86 (2023).
46. Shull, J. M., Danforth, C. W. Distances to Galactic OB Stars: Photometry versus Parallax, The Astrophysical Journal, 882, 180 (2019).
47. Witt, A. N., Gordon, K. D. Multiple Scattering in Clumpy Media. II. Galactic Environments, The Astrophysical Journal, 528, 799-816 (2000).
48. Scicluna, P., Siebenmorgen, R. Extinction and dust properties in a clumpy medium, Astronomy and Astrophysics, 584, A108 (2015).
49. Wang, L. Dust around Type Ia Supernovae, The Astrophysical Journal, 635, L33-L36 (2005).

Appendix A: Extended data

The supporting data of Fig. 1 and Fig. 3 are compiled in Table 1. We specify the spectral-type and luminosity class (SpL) of the primary star, and if available, those of the binary. We give the absolute magnitude M_{V}, the V-band magnitude, an identifier (V[11], F[12], G[13]) for the refernces pertaining to the employed reddening curve used and the associated visual extinction $A_{\mathrm{V}}^{\mathrm{Ref}}$, which is from the same references. The latter is used to compute the luminosity distance $D_{\mathrm{L}}^{\mathrm{Ref}}$. Further we specify, the distance derived from the GAIA parallax, D_{GAIA} with 1σ error. The last two columns of Table 1 present our luminosity distance D_{L} derived utilizing A_{V} as obtained from Eq. 1.

The absolute magnitudes M_V by (40) are used and complemented by (41). The offset between both catalogues depends on the luminosity class and is for (V, III, Ia, Ib) stars typically $\sigma_C = (0.05, 0.25, 0.22, 0.18)$, repectively. The indices and suffixes within the table relate to the uncertainties at a 1σ level in M_V and the corresponding error in $D_{\mathrm{L}}^{\mathrm{Ref}}$.

For instance, the positive error in M_V for the B3V star HD 027778 is calculated by considering $\sigma_{\mathrm{SpT}}(M_V(B3V), M_V(B3.5V)) = [-1.52, -1.48] = 0.04$, $\sigma_{\mathrm{LC}}(M_V(B3V), M_V(B3IV)) = [-1.52, -2.3] = 0.78$ and $\sigma_C(V) = 0.056$, and subsequently combining these factors in quadrature, yielding $\sigma = 0.395$. A similar methodology is applied to calculate the negative deviation by using the next lower spectral type and luminosity class. In the context of binary systems, we convert M_V to intensities for both stars, then convert the sum of these intensities back to the magnitude of the combined system.

Table A.1. Data supporting Fig. 1 and Fig. 3.

Star	SpL	M_V (mag)	V (mag)	Ref.	A_V^{Ref} (mag)	D_L^{Ref} (pc)	D_{GAIA} (pc)	D_L (pc)	A_V (mag)
HD 027778	B3V	$-1.52^{0.39}_{-0.44}$	6.33	G	1.09	225^{45}_{-41}	212 ± 1	212	1.22
HD 030470	B9V	$0.10^{0.23}_{-0.27}$	9.47	F	1.08	455^{51}_{-53}	542 ± 15	483	0.95
HD 030492	A0III	$-0.09^{0.69}_{-0.41}$	8.97	F	1.17	378^{143}_{-65}	437 ± 8	409	1.00
HD 037903	B2V	$-2.28^{0.46}_{-0.46}$	7.84	G	1.49	532^{124}_{-101}	399 ± 4	399	2.11
HD 038023	B3V	$-1.52^{0.39}_{-0.44}$	8.87	F	1.64	562^{112}_{-103}	417 ± 3	417	2.29
HD 046149	O8V+B0.5V	$-4.95^{0.48}_{-0.43}$	7.62	F	1.29	1803^{447}_{-327}	1566 ± 79	1566	1.60
HD 046202	O9V	$-4.30^{0.27}_{-0.27}$	8.24	G	1.53	1592^{208}_{-184}	1411 ± 228	1411	1.79
HD 046223	O4V	$-5.65^{0.13}_{-0.13}$	7.31	V	1.48	1977^{126}_{-118}	1435 ± 54	1435	2.18
HD 047382	B0III+SB	$-5.00^{0.42}_{-0.30}$	7.14	F	1.37	$> 1426^{306}_{-182}$	961 ± 72	961	2.23
HD 054439	B1V	$-3.04^{0.50}_{-0.53}$	7.71	F	0.80	977^{254}_{-211}	1030 ± 40	1007	0.73
HD 062542	B5V	$-1.21^{0.12}_{-0.09}$	7.99	G	1.16	406^{23}_{-16}	367 ± 2	367	1.38
HD 070614	B3III	$-2.85^{0.85}_{-0.33}$	9.29	F	2.14	1000^{478}_{-139}	1532 ± 30	1219	1.71
HD 091824	O7V	$-4.90^{0.21}_{-0.21}$	8.15	F	0.77	2858^{293}_{-266}	1859 ± 97	1859	1.70
HD 092044	B1Ib	$-5.95^{0.59}_{-0.46}$	8.31	F	1.42	3698^{1152}_{-712}	2378 ± 125	2378	2.38
HD 093205	O4V+O8V	$-6.00^{0.27}_{-0.27}$	7.75	V	1.23	3191^{429}_{-378}	2322 ± 134	2322	1.92
HD 093222	O7III	$-5.70^{0.11}_{-0.22}$	8.10	G	1.76	2559^{130}_{-242}	2438 ± 136	2117	2.17
HD 096675	B7V	$-0.67^{0.15}_{-0.15}$	7.68	G	0.99	296^{21}_{-20}	162 ± 1	162	2.30
HD 101008	B0III	$-5.00^{0.42}_{-0.30}$	9.16	F	0.93	4426^{949}_{-566}	2450 ± 117	2449	2.21
HD 108927	B5V	$-1.21^{0.12}_{-0.09}$	7.77	F	0.74	445^{25}_{-18}	336 ± 3	336	1.35
HD 110336	B8V	$-0.49^{0.20}_{-0.14}$	8.64	F	1.21	384^{38}_{-25}	310 ± 1	310	1.68
HD 110715	B9III	$-0.77^{0.27}_{-0.50}$	8.67	F	1.31	423^{56}_{-88}	525 ± 9	456	1.15
HD 110946	B2III	$-3.55^{0.60}_{-0.29}$	9.18	F	1.60	1683^{537}_{-207}	2110 ± 54	1873	1.37
HD 112607	B5III	$-1.48^{0.42}_{-0.29}$	8.10	F	0.85	557^{120}_{-69}	594 ± 7	588	0.73
HD 112954	B9III	$-0.77^{0.27}_{-0.50}$	8.39	F	1.75	303^{40}_{-63}	383 ± 3	338	1.52
HD 129557	B1V	$-3.04^{0.50}_{-0.53}$	6.09	V	0.53	525^{136}_{-113}	413 ± 6	413	1.05
HD 146284	B9III	$-0.77^{0.27}_{-0.50}$	6.71	F	0.77	220^{29}_{-46}	204 ± 1	204	0.93
HD 146285	B9IV	$0.10^{0.22}_{-0.26}$	7.93	F	1.23	209^{23}_{-24}	156 ± 1	156	1.87
HD 147196	B8V	$-0.49^{0.20}_{-0.14}$	7.04	F	0.84	218^{21}_{-14}	138 ± 1	138	1.83
HD 148579	B9IV	$0.10^{0.22}_{-0.26}$	7.35	F	1.40	148^{16}_{-17}	140 ± 2	140	1.51
HD 148594	B7V	$-0.67^{0.15}_{-0.15}$	6.89	F	0.65	241^{17}_{-16}	183 ± 1	183	1.24
HD 152245	B0.5III	$-4.80^{0.45}_{-0.32}$	8.39	V	1.08	2642^{601}_{-358}	1859 ± 102	1858	1.84
HD 152249	O9Ia	$-7.00^{0.46}_{-0.46}$	6.38	G	1.58	2291^{536}_{-434}	1547 ± 55	1547	2.43
HD 156247	B5III+B5V	$-2.11^{0.46}_{-0.32}$	5.91	F	0.73	287^{67}_{-39}	236 ± 5	236	1.15
HD 164402	B0Ib+SB	$-6.17^{0.47}_{-0.25}$	5.74	V	0.70	$> 1746^{422}_{-191}$	749 ± 83	749	2.54
HD 167264	B0Ib+B0V	$-6.29^{0.58}_{-0.42}$	5.34	V	0.98	1350^{411}_{-237}	1140 ± 217	1140	1.35
HD 167771	O6III+O8III	$-6.47^{0.32}_{-0.40}$	6.52	G	1.48	2005^{317}_{-334}	1560 ± 79	1559	2.03
HD 168076	O4III	$-6.20^{0.13}_{-0.16}$	8.23	G	2.61	2312^{145}_{-166}	1091 ± 330	1091	4.24
HD 170634	B8V	$-0.49^{0.20}_{-0.14}$	9.85	F	2.05	455^{45}_{-29}	438 ± 3	438	2.13
HD 170740	B2V	$-2.28^{0.46}_{-0.46}$	5.75	F	1.37	215^{50}_{-41}	226 ± 4	226	1.26
HD 185418	B0.5V	$-3.55^{0.42}_{-0.36}$	7.49	G	1.39	851^{180}_{-131}	707 ± 10	707	1.79
HD 287150	A1III	$0.73^{1.06}_{-0.36}$	9.26	F	1.22	290^{183}_{-44}	404 ± 3	314	1.04
HD 294304	B6V	$-0.89^{0.14}_{-0.15}$	10.05	F	1.23	875^{58}_{-59}	755 ± 11	755	1.55
HD 303308	O6V	$-5.20^{0.19}_{-0.19}$	8.12	V	1.36	2466^{220}_{-202}	2257 ± 108	2257	1.55
HD 315021	B0V	$-3.85^{0.34}_{-0.34}$	8.57	F	1.24	1722^{288}_{-247}	1438 ± 72	1438	1.63

Table A.1. – continued —

Star	SpL	M_V (mag)	V (mag)	Ref.	A_V^{Ref} (mag)	D_L^{Ref} (pc)	D_{GAIA} (pc)	D_L (pc)	A_V (mag)
HD 315023	B2V	$-2.28^{0.46}_{-0.46}$	10.03	F	1.48	1466^{342}_{-277}	1294 ± 38	1294	1.75
HD 315024	B1V	$-3.04^{0.50}_{-0.53}$	9.63	F	1.20	1968^{510}_{-425}	1349 ± 46	1349	2.02
HD 315032	B1V	$-3.04^{0.50}_{-0.53}$	9.18	F	1.01	1746^{453}_{-377}	1379 ± 57	1379	1.52

Notes: SB denotes spectroscopic binary.

Table A.2. Model parameters.

Star	m_{μ}	$m_{\rm Si}$	$m_{\rm vSi}$	$m_{\rm aC}$	$m_{\rm vgr}$	$m_{\rm PAH}$	x_0 (μm^{-1})	γ	q	r^+_{μ} (μm^{-1})	$r^+_{\rm Si}$ (nm)	$r^+_{\rm aC}$ (nm)	χ^2_r
HD 027778	34.8	31.2	21.8	7.1	2.5	2.5	4.59	1.85	2.37	2.1	222	201	0.3
HD 030470	–	45.6	32.8	15.9	4.0	1.6	4.59	0.62	2.35	1.6	222	211	0.5
HD 030492	–	49.2	32.4	13.2	3.6	1.6	4.59	0.62	2.49	1.6	222	245	0.3
HD 037903	56.7	16.9	10.5	12.5	2.0	1.4	4.60	1.27	2.28	1.3	257	201	0.3
HD 038023	49.1	24.2	13.3	9.8	1.4	2.2	4.57	1.72	2.38	1.4	222	201	0.5
HD 046149	29.9	36.8	19.4	8.4	4.1	1.4	4.60	0.54	2.35	0.8	233	158	0.5
HD 046202	30.6	46.1	14.5	4.6	0.6	3.6	4.63	0.89	2.64	1.1	270	201	0.2
HD 046223	54.2	24.0	14.6	4.4	0.9	1.9	4.66	0.95	2.32	2.2	233	211	0.4
HD 047382	62.8	24.4	6.9	3.8	1.5	0.7	4.58	0.70	2.50	1.7	233	233	8.8
HD 054439	–	56.7	22.7	13.2	5.5	2.0	4.60	0.50	2.33	1.6	222	201	0.7
HD 062542	29.0	30.3	30.4	6.9	1.7	1.7	4.64	2.00	2.60	1.2	233	211	0.3
HD 070614	5.8	58.7	16.9	10.6	4.7	3.3	4.57	0.66	2.36	1.6	233	233	0.5
HD 091824	86.8	6.2	3.1	3.2	0.4	0.2	4.65	0.66	2.38	3.9	222	192	1.0
HD 092044	85.6	5.8	4.5	2.9	0.4	0.7	4.62	1.80	2.32	6.8	245	211	0.4
HD 093205	56.3	20.3	13.3	7.6	1.3	1.2	4.61	1.24	2.32	1.6	222	211	0.5
HD 093222	60.7	17.3	6.7	13.0	1.2	1.2	4.57	0.72	2.62	1.6	270	211	2.5
HD 096675	76.1	9.6	7.7	3.4	1.0	2.3	4.56	1.95	2.30	1.8	222	211	0.3
HD 101008	80.7	10.5	4.1	3.5	0.9	0.3	4.60	0.69	2.07	2.1	257	211	1.2
HD 108927	91.5	4.6	2.3	1.0	0.5	0.2	4.60	0.87	1.85	9.0	270	201	0.9
HD 110336	72.4	11.6	10.0	3.6	1.3	1.0	4.60	2.00	1.99	6.4	222	211	0.7
HD 110715	–	43.1	38.6	11.6	4.8	1.8	4.57	0.81	2.04	1.6	211	222	0.3
HD 110946	–	41.6	27.3	23.3	3.8	4.0	4.58	1.16	2.83	1.6	201	283	0.5
HD 112607	–	51.0	33.5	8.6	4.6	2.2	4.55	0.70	2.27	1.6	222	344	1.1
HD 112954	–	41.3	40.5	11.9	3.8	2.5	4.57	1.10	2.58	1.6	233	257	0.5
HD 129557	73.6	18.5	4.5	0.7	1.5	1.2	4.55	0.77	1.70	2.7	257	211	1.1
HD 146284	33.1	33.9	15.4	12.1	2.9	2.6	4.56	0.86	2.02	1.3	233	201	0.5
HD 146285	60.3	22.3	6.2	7.8	1.8	1.5	4.56	0.77	1.73	1.3	257	201	0.4
HD 147196	78.7	10.2	6.4	2.6	0.4	1.6	4.63	1.49	1.71	2.4	245	222	0.6
HD 148579	29.1	33.8	14.0	17.9	2.7	2.4	4.55	0.84	1.96	1.1	245	211	0.3
HD 148594	68.1	20.4	5.4	4.0	1.3	0.8	4.53	0.66	1.75	1.3	245	192	0.4
HD 152245	64.6	16.6	8.4	8.2	0.9	1.2	4.62	0.70	2.42	1.6	201	174	0.4
HD 152249	62.3	18.9	7.3	9.0	1.5	0.9	4.60	0.91	2.49	1.4	211	183	0.4
HD 156247	60.7	23.4	8.8	3.9	2.0	1.0	4.58	0.65	2.02	1.6	257	166	0.3
HD 164402	86.0	9.1	2.7	1.2	0.6	0.4	4.58	0.78	2.07	1.9	245	211	0.5
HD 167264	48.4	27.2	10.4	10.0	2.3	1.7	4.60	0.85	2.15	1.3	245	192	0.3
HD 167771	50.2	24.6	9.6	11.8	2.1	1.6	4.56	0.70	2.33	1.0	222	183	0.6
HD 168076	63.3	16.5	5.9	12.1	0.5	1.8	4.63	0.95	2.71	1.3	245	192	1.6
HD 170634	89.5	4.8	3.5	1.3	0.2	0.6	4.61	1.36	2.31	104	257	201	0.4
HD 170740	7.1	49.9	24.2	12.5	4.1	2.4	4.59	0.80	2.63	1.6	233	211	0.4
HD 185418	50.8	34.5	7.8	2.4	0.4	4.1	4.64	1.02	2.34	2.4	257	201	0.4
HD 287150	8.6	34.4	32.2	19.5	2.7	2.6	4.55	0.83	2.88	1.6	233	211	0.6
HD 294304	55.6	19.5	11.9	9.6	1.5	1.9	4.55	1.12	2.85	4.8	257	201	0.3
HD 303308	71.1	15.7	7.9	3.4	0.4	1.5	4.64	1.13	2.36	11	257	211	0.4
HD 315021	50.0	27.5	8.3	10.6	2.4	1.2	4.57	0.55	1.86	1.5	270	192	0.3
HD 315023	34.9	34.9	8.0	18.1	1.9	2.2	4.57	0.77	2.67	0.8	283	211	0.6
HD 315024	69.5	14.5	5.9	7.9	1.4	0.9	4.59	0.75	2.43	1.6	245	201	0.4
HD 315032	73.9	12.1	5.9	6.1	1.5	0.5	4.58	0.57	2.29	3.1	245	211	0.4